Commun Transp Res

Research Article

Integrated vehicle and bidirectional charging scheduling for V2G-enabled electric bus system

Yiming Bie[1], Yuman Xu[1], Ao Xue[1], Jinhua Ji[1,✉], Menglin Yang[2], Jue Zhou[1]

Cite this article: https://doi.org/10.26599/COMMTR.2026.9640064

ABSTRACT: Electric bus (EB) fleets are transformed into flexible energy resources through vehicle-to-grid (V2G) technology while maintaining regular transit services. This paper investigates the joint optimization of vehicle operations and bidirectional charging decisions for a multi-route EB system with limited bidirectional and unidirectional chargers. A time-expanded network is constructed to capture EB's daily operations, supporting optimization of partial charging and discharging decisions. Considering the effect of upward and downward regulation demands of the power grid, a mixed-integer programming model is established to minimize operating costs and regulation deviation. Then, a column-generation-based diving heuristic algorithm incorporating two dominance strategies is further designed to efficiently search for a high-quality solution. Finally, numerical experiments based on real-world bus routes are conducted, and results indicate that the optimized scheme enhances both the economic performance and grid-friendly operation of the EB system. Specifically, the discharging revenues effectively offset the electricity purchase and battery degradation costs, while the EB fleet meets 86.3% of the regulation demand. In addition, the two dominance strategies reveal different advantages, dominance strategy I reduces total costs by 28.7 CNY, whereas dominance strategy II shortens the solution time by 39.6%.

KEYWORDS: electric bus; vehicle-to-grid; vehicle scheduling; diving heuristic; regulation demand

1 Introduction

1.1. Background

With the growing emphasis on sustainable and low-carbon mobility, the electrification of public transit systems has continued to accelerate. Electric buses (EBs) have gained a prominent position of this transition because they can reduce greenhouse gas emissions and noise pollution. Beyond these environmental benefits, the batteries carried by EBs also provide considerable potential for energy storage and power grid support. As EB deployment expands and charging technologies continue to develop, EBs are gradually transforming from passive electricity consumers into flexible energy storage resources. Vehicle-to-grid (V2G) technology facilitates this evolution by allowing energy to flow bidirectionally between EB batteries and the power grid (Zeng and Qu, 2023; Shaheen et al., 2024; Li et al., 2026a).

Compared with private electric vehicles, EB fleets are particularly suitable for V2G applications. They are typically managed centrally (Bie et al., 2024), operate on regular timetables and scheduling schemes (Cong et al., 2025), rely on depot-based charging infrastructure (Dong et al., 2024), and have relatively predictable idle periods (Yao et al., 2025). These characteristics create favorable conditions for aggregating dispersed batteries and scheduling them as a controllable resource for the power grid. Beyond this theoretical potential, V2G demonstration projects in cities such as Shanghai, New York, and London have also provided practical evidence of technical feasibility.

The integration of V2G into EB operations may create benefits for both transit operators and the power grid. For transit operators, bidirectional charging may create revenue through energy arbitrage, thereby improving the economic sustainability of EB systems. For the power grid, aggregated EB batteries can serve as flexible resources to support peak shaving and reserve service, compensating for the limited regulation capability of conventional generation units. However, these potential benefits introduce additional operational challenges. Supplying electricity back to the power grid may reduce the available state of charge (SOC) of EBs before subsequent trips, increasing the risk of service infeasibility (Zhou et al., 2025a) and imposing stricter requirements on charging coordination (Ji et al., 2026a). The additional energy throughput (Sagaria et al., 2025) may accelerate battery aging and increase battery degradation costs (Othman et al., 2025).

These issues become more challenging in the multi-route EB system (Cong et al., 2024), where bus assignments, trip operations, battery energy management (Jiang et al., 2022a), and allocation of limited bidirectional and unidirectional chargers are highly interdependent (Wang et al., 2024). Motivated by these challenges, this paper develops vehicle scheduling and bidirectional charging scheduling for a multi-route EB system, aiming to ensure normal transit service while exploiting the economic and grid-friendly potential enabled by V2G technology.

1.2. Literature review

Research on the vehicle scheduling problem for EBs (E-VSP) has been conducted on the system equipped with unidirectional chargers, hereafter referred to as E-VSP-UC, where EBs draw energy from the power grid to meet daily service requirements. Enabled by V2G technology, the system equipped with bidirectional chargers allows EBs to exchange

[1] School of Transportation, Jilin University, Changchun 130022, China. [2] Institute of Traffic Telematics, Technische Universität Dresden, Dresden 01069, Germany.

✉ Corresponding author. E-mail: jinhua_ji@126.com

Received: August 10, 2026; Revised: September 20, 2026; Accepted: October 27, 2026

© The Author(s) 2026. This is an open access article under the terms of the Creative Commons Attribution 4.0 International License (CC BY 4.0, http://creativecommons.org/licenses/by/4.0/).

Just Accepted

energy with the power grid, giving rise to E-VSP-BC. Accordingly, this section classifies existing studies according to the type of chargers and reviews them separately.

(i) E-VSP-UC

Studies on E-VSP-UC optimize vehicle assignment and charging decisions (Huang et al., 2026), typically with the objective of reducing fleet size (Xu et al., 2023), operating costs (Whitaker et al., 2023), or charging costs (Teng et al., 2020). These studies have provided important modeling and algorithmic foundations for improving the economic performance of EB systems (Ji et al., 2026b; Zeng et al., 2023a).

In single-route settings, EBs are assigned to scheduled trips, while charging decisions are arranged during idle periods to maintain service integrity. A typical formulation incorporates core operational constraints (Li et al., 2026b), including trip coverage, flow conservation (Zeng et al., 2023b), energy feasibility (Zhang et al., 2023), and charging duration (Ji et al., 2023). Building on this basic framework, existing studies have extended the problem in several directions. Various charging modes have been investigated, including opportunity and overnight charging (Abdelwahed et al., 2020; Tang et al., 2024), partial and full charging (Lian et al., 2023; Xiong et al., 2022), as well as depot-based and en-route charging (Wang et al., 2023; Zeng et al., 2024). Time-of-use electricity prices have also been considered to guide charging activities toward low-price periods (Zhang et al., 2024a) and reduce electricity expenditure (He et al., 2022; Zhao et al., 2025). Operational uncertainties, including uncertain travel times (Tang et al., 2019) and stochastic energy consumption (Qiu et al., 2026), have also been modeled to improve departure punctuality and energy reliability of the EB system. Nevertheless, many of them assume that charging resources are sufficient, which overlooks the impacts of charger competition.

As the problem scale expands from a single route to multiple routes, studies on E-VSP-UC place greater emphasis on the coordinated use of limited chargers (Jiang et al., 2022b; Zhang et al., 2024b; Jia and An, 2025). In multi-route settings, EB serving different routes may arrive at depots or charging stations during overlapping time periods, resulting in charger competition and charging delays. To capture the operational restrictions imposed by shared chargers, existing studies have incorporated depot capacity (Jahic et al., 2021), charging time windows (Gkiotsalitis et al., 2023), deadheading costs, and waiting delays into scheduling models (Lacombe et al., 2024). These studies have provided a realistic framework for managing shared charging resources. However, they generally treat EBs solely as electricity consumers and do not consider discharging energy back to the power grid.

(ii) E-VSP-BC

E-VSP-BC extends E-VSP-UC by incorporating discharging decisions and allowing EBs to exchange energy bidirectionally with the power grid. Related formulations have been examined by Zhou et al. (2025b) and Son et al. (2025), with similar V2G settings also considered by Kang et al. (2025) and Najafi et al. (2025). Research efforts focused on the economic and operational implications from several perspectives. For example, some studies have conducted cost-benefit analyses of V2G integration by comparing V2G-capable EBs with fueled buses or diesel buses (Shirazi et al., 2015; Zheng et al., 2026). Other studies have examined how battery-swapping EBs can participate in wholesale electricity (Brinkel et al., 2023; Ke et al., 2020) and ancillary service markets (Zhou et al., 2024; Yang et al., 2021). Battery degradation has also been incorporated to capture aging costs (Li et al., 2025) caused by more frequent charging and discharging (Manzolli et al., 2022). They have demonstrated potential benefits of integrating V2G technology into EB operations and have provided useful insights into the trade-offs among operating costs, discharging revenues, and battery degradation costs.

Most studies are conducted in single-route settings and assume that the depot is equipped with sufficient and homogeneous bidirectional chargers, neglecting resource competition in multi-route shared-depot operations. In addition, charging modes are often simplified or limited to full charging, leaving the flexibility offered by partial charging and discharging insufficiently explored. Moreover, power grid regulation demands are rarely incorporated into scheduling models, limiting the evaluation of EB fleets as grid-friendly flexible resources.

1.3. Contributions

This paper develops a coordinated optimization framework for V2G-enabled multi-route EB systems, determining vehicle operation and bidirectional charging scheme, while demonstrating the potential of EBs as flexible energy storage resources. The contributions are summarized as follows:

i) A time-expanded network is constructed to capture the daily operation process of EBs, including trip execution, waiting, charging, and discharging activities. Based on this network, the integrated scheduling problem is transformed into a path-selection problem, which enables optimization of partial charging and discharging decisions.

ii) Considering the effect of upward and downward regulation demands of the power grid, a vehicle scheduling and bidirectional charging scheduling model subject to depot capacity constraints is developed. The model is constructed as a mixed-integer program to minimize operating costs and regulation deviation penalty costs. This captures the trade-off between economic performance and grid-friendly operations of EBs.

iii) A column-generation-based diving heuristic algorithm is developed with two dominance strategies. The algorithm combines the ability of column generation in handling large-scale optimization problems with the advantage of the diving heuristic in efficiently obtaining a high-quality feasible solution.

The paper is structured as follows. The integrated vehicle and bidirectional charging scheduling model is formulated in Section 2, together with the column-generation-based diving heuristic developed for its solution. Numerical experiments are presented in Section 3, where comparative and sensitivity analyses are also conducted. Section 4 summarizes the major findings and discusses potential avenues for further research.

2 Methodology

2.1. Time-expanded network construction

Multiple bus routes share a depot for both charging from and discharging to the power grid in the V2G-enabled EB system. Let N and H represent the numbers of unidirectional and bidirectional chargers at the depot, respectively. Let P_1^{cha} and P_2^{dis} denote the charging power drawn by EBs from the power grid and the discharging power delivered back. The set of bus routes originating from the depot is represented by L. D_l^{dh} and W_l^{dh} indicate the deadheading time and energy consumption between the depot and the origin station, respectively. The EB fleet is organized on a route basis, with a predefined set of buses assigned to each route. The operational coupling among routes mainly arises from their shared charging and discharging resources at the depot. For each

Under Review

route l, the corresponding set of EBs is denoted by K_l, with Q_l characterizing their battery rated capacity and c_0^{bat} representing the degradation cost associated with a unit throughput in battery energy. Let B_l denote the set of trips on route l. For trip $b \in \mathrm{B}_l$, $T_{l,b}^{\mathrm{sta}}$ is used to represent the scheduled departure time. The associated travel time and energy consumption are characterized by $D_{l,b}^{\mathrm{dri}}$ and $W_{l,b}^{\mathrm{dri}}$.

The scheduling horizon is discretized into F periods. For period f, T_f^{sta} indicates its starting time, whereas T_f^{end} denotes the corresponding ending time. The electricity purchase price and resale price in period f are denoted as c_f^{cha} and c_f^{dis}. For each regulation period f, the upward and downward regulation energy demands assigned by the power grid to the depot are denoted by w_f^+ and w_f^-. Upward regulation is realized by supplying energy from the EB fleet to the power grid through discharging, whereas downward regulation is realized by absorbing energy from the power grid through charging. The corresponding regulation energy is determined by the charging or discharging power and the associated duration.

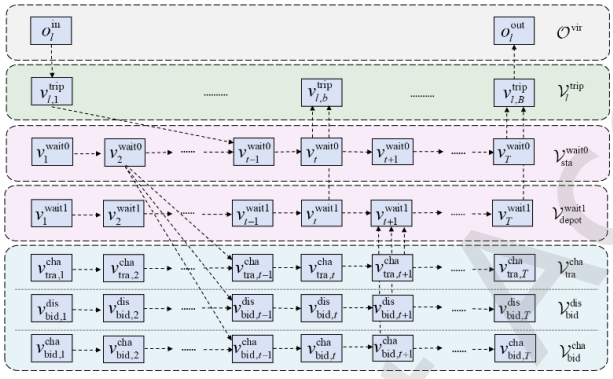


Fig. 1. Schematic representation of the time-expanded network.

The scheduling horizon is discretized into time slots of length Δt. Let T denote the set of time points, where t denotes the corresponding time index. Based on this discretization, a time-expanded network $\mathrm{G}=(\mathrm{V},\mathrm{A})$ is developed, as shown in Fig. 1, where A represents the arc set and V defines the node set. Each arc connects two distinct nodes i and j in V. As defined in Eq. (1), V comprises virtual origin and destination nodes $\mathrm{O}^{\mathrm{vir}}$, trip nodes on route l $\mathrm{V}_l^{\mathrm{trip}}$, waiting nodes at the origin station $\mathrm{V}_{\mathrm{sta}}^{\mathrm{wait0}}$, waiting nodes at the depot $\mathrm{V}_{\mathrm{depot}}^{\mathrm{wait1}}$, charging nodes associated with unidirectional chargers $\mathrm{V}_{\mathrm{tra}}^{\mathrm{cha}}$ and bidirectional chargers $\mathrm{V}_{\mathrm{bid}}^{\mathrm{cha}}$, and discharging nodes for bidirectional chargers $\mathrm{V}_{\mathrm{bid}}^{\mathrm{dis}}$. Waiting nodes are explicitly introduced to keep the arc set manageable. Without waiting nodes, each trip node would need to be connected directly to all reachable charging and discharging nodes to represent the dwell time of an EB at the depot, resulting in a much denser network. With waiting nodes, dwell time can be represented by arcs between consecutive time points, which reduces the number of required arcs.

$$
\begin{aligned}
\mathrm{V} &= \mathrm{O}^{\mathrm{vir}} \cup \mathrm{V}_l^{\mathrm{trip}} \cup \mathrm{V}_{\mathrm{sta}}^{\mathrm{wait0}} \cup \mathrm{V}_{\mathrm{depot}}^{\mathrm{wait1}} \cup \mathrm{V}_{\mathrm{tra}}^{\mathrm{cha}} \cup \mathrm{V}_{\mathrm{bid}}^{\mathrm{cha}} \cup \mathrm{V}_{\mathrm{bid}}^{\mathrm{dis}} \\
&= \left\{ o_l^{\mathrm{in}},\ o_l^{\mathrm{out}} \middle| \forall l \in \mathrm{L} \right\} \cup \left\{ v_{l,b}^{\mathrm{trip}} \middle| \forall l \in \mathrm{L},\ b \in \mathrm{B}_l \right\} \\
&\cup \left\{ v_t^{\mathrm{wait0}},\ v_t^{\mathrm{wait1}},\ v_{\mathrm{tra},t}^{\mathrm{cha}},\ v_{\mathrm{bid},t}^{\mathrm{cha}},\ v_{\mathrm{bid},t}^{\mathrm{dis}} \middle| t \in \mathrm{T} \right\}
\end{aligned} \tag{1}
$$

where o_l^{in} and o_l^{out} denote the virtual origin and destination nodes of route l. All EBs assigned to route l depart from o_l^{in} and eventually return to o_l^{out}; $v_{l,b}^{\mathrm{trip}}$ denotes the service node of trip b on route l. At time t, v_t^{wait0} and v_t^{wait1} represent the waiting nodes at the origin station and the depot at time t; $v_{\mathrm{tra},t}^{\mathrm{cha}}$ is the charging node of unidirectional chargers, whereas $v_{\mathrm{bid},t}^{\mathrm{cha}}$ and $v_{\mathrm{bid},t}^{\mathrm{dis}}$ denote the charging and discharging nodes of bidirectional chargers.

The network shown in Fig. 1 contains several representative arc categories: pull-in arcs, pull-out arcs, departure and arrival arcs of trips, waiting arcs, charging arcs associated with unidirectional or bidirectional chargers, discharging arcs associated with bidirectional chargers, and access and egress arcs of charging or discharging activities. For any arc connecting nodes i and j, the energy variation coefficient $w(i,j)$ and the cost coefficient $c(i,j)$ are defined as follows:

i) Pull-in arcs $\mathrm{A}_l^{\mathrm{in}}$: It represents the transition of EB b from the virtual origin of route l to its first assigned trip. It represents the initial deadheading movement from the depot to origin station. Accordingly, $w\left(o_l^{\mathrm{in}},\ v_{l,b}^{\mathrm{trip}}\right) = -W_l^{\mathrm{dh}}$ and $c\left(o_l^{\mathrm{in}},\ v_{l,b}^{\mathrm{trip}}\right) = c_0^{\mathrm{bat}} W_l^{\mathrm{dh}}$.

ii) Pull-out arcs $\mathrm{A}_l^{\mathrm{out}}$: It connects the last trip served by EB b to the virtual destination node of route l. It represents the final deadheading movement from the origin station back to depot after the EB completes its daily service. In this case, $w\left(v_{l,b}^{\mathrm{trip}},\ o_l^{\mathrm{out}}\right) = -W_l^{\mathrm{dh}}$ and $c\left(v_{l,b}^{\mathrm{trip}},\ o_l^{\mathrm{out}}\right) = c_0^{\mathrm{bat}} W_l^{\mathrm{dh}}$.

iii) Departure arcs of trips from the origin station $\mathrm{A}_{\mathrm{trip}}^{\mathrm{wait0}}$: These arcs describe the transition of an EB from the waiting state at the origin station to the trip service state ($t = T_{l,b}^{\mathrm{sta}}$). This process does not involve any energy variation. Therefore, $w\left(v_t^{\mathrm{wait0}},\ v_{l,b}^{\mathrm{trip}}\right) = 0$ and $c\left(v_t^{\mathrm{wait0}},\ v_{l,b}^{\mathrm{trip}}\right) = 0$.

iv) Departure arcs of trips from the depot $\mathrm{A}_{\mathrm{trip}}^{\mathrm{wait1}}$: These arcs link the waiting state at the depot to the trip service state, reflecting the deadheading movement from the depot. Hence, $w\left(v_t^{\mathrm{wait1}},\ v_{l,b}^{\mathrm{trip}}\right) = -W_l^{\mathrm{dh}}$ and $c\left(v_t^{\mathrm{wait1}},\ v_{l,b}^{\mathrm{trip}}\right) = c_0^{\mathrm{bat}} W_l^{\mathrm{dh}}$.

v) Arrival arcs of trips $\mathrm{A}_{\mathrm{wait}}^{\mathrm{trip}}$: They indicate the completion of a trip and the transition to the waiting state at the origin station, $w\left(v_{l,b}^{\mathrm{trip}},\ v_t^{\mathrm{wait0}}\right) = -W_{l,b}^{\mathrm{dri}}$ and $c\left(v_{l,b}^{\mathrm{trip}},\ v_t^{\mathrm{wait0}}\right) = c_0^{\mathrm{bat}} W_{l,b}^{\mathrm{dri}}$.

vi) Waiting arcs $\mathrm{A}_{\mathrm{wait}}^{\mathrm{wait}}$: Waiting arcs capture the time spent by an EB in the waiting state at either the depot or the origin station. Since no energy is consumed or replenished, $w\left(v_t^{\mathrm{wait0}},\ v_{t+1}^{\mathrm{wait0}}\right) = w\left(v_t^{\mathrm{wait1}},\ v_{t+1}^{\mathrm{wait1}}\right) = 0$ and $c\left(v_t^{\mathrm{wait0}},\ v_{t+1}^{\mathrm{wait0}}\right) = c\left(v_t^{\mathrm{wait1}},\ v_{t+1}^{\mathrm{wait1}}\right) = 0$.

vii) Charging arcs for unidirectional chargers $\mathrm{A}_{\mathrm{tra}}^{\mathrm{cha}}$: The charging duration associated with a unidirectional charger is

Just Accepted

represented through these arcs. Over one interval Δt, the battery energy increases by $P_1^{\text{cha}}\Delta t$, while the corresponding cost consists of electricity purchase costs $c_f^{\text{cha}}P_1^{\text{cha}}\Delta t$ and battery degradation costs $c_0^{\text{bat}}P_1^{\text{cha}}\Delta t$. Where c_f^{cha} applies to any period f satisfying $t \geq T_f^{\text{sta}}$ and $t+1 \leq T_f^{\text{end}}$.

viii) Charging arcs for bidirectional chargers $\text{A}_{\text{bid}}^{\text{cha}}$: Charging activities performed through bidirectional chargers are modeled by this arc set. It produces the same energy increment and costs over Δt as those for unidirectional chargers.

ix) Discharging arcs for bidirectional chargers $\text{A}_{\text{bid}}^{\text{dis}}$: This arc set represents the duration of discharging operations. During one interval Δt, the battery energy decreases by $P_2^{\text{dis}}\Delta t$, while the corresponding cost consists of discharging revenues $-c_f^{\text{dis}}P_2^{\text{dis}}\Delta t$ and battery degradation costs $c_0^{\text{bat}}P_2^{\text{dis}}\Delta t$.

x) Access arcs of charging or discharging $\text{A}_{\text{pile}}^{\text{wait}}$: Access arcs model the transition from the waiting state at the origin station to either a charging or a discharging state. To initiate such an activity, the EB must deadhead from the origin station to the depot. Let $D_{\min}^{\text{pile}}$ denote the minimum charging or discharging duration.

For charging access arcs, $w\left(v_t^{\text{wait0}},\ v_{\text{tra},t+D_l^{\text{dh}}+D_{\min}^{\text{pile}}}^{\text{cha}}\right)=w\left(v_t^{\text{wait0}},\ v_{\text{bid},t+D_l^{\text{dh}}+D_{\min}^{\text{pile}}}^{\text{cha}}\right)=-W_l^{\text{dh}}+P_1^{\text{cha}}D_{\min}^{\text{pile}}$ and $c\left(v_t^{\text{wait0}},\ v_{\text{tra},t+D_l^{\text{dh}}+D_{\min}^{\text{pile}}}^{\text{cha}}\right)=c\left(v_t^{\text{wait0}},\ v_{\text{bid},t+D_l^{\text{dh}}+D_{\min}^{\text{pile}}}^{\text{cha}}\right)=c_f^{\text{cha}}P_1^{\text{cha}}D_{\min}^{\text{pile}}+c_0^{\text{bat}}\left(P_1^{\text{cha}}D_{\min}^{\text{pile}}+W_l^{\text{dh}}\right)$. For discharging access arcs, $w\left(v_t^{\text{wait0}},\ v_{\text{bid},t+D_l^{\text{dh}}+D_{\min}^{\text{pile}}}^{\text{dis}}\right)=-W_l^{\text{dh}}-P_2^{\text{dis}}D_{\min}^{\text{pile}}$ and $c\left(v_t^{\text{wait0}},\ v_{\text{bid},t+D_l^{\text{dh}}+D_{\min}^{\text{pile}}}^{\text{dis}}\right)=-c_f^{\text{dis}}P_2^{\text{dis}}D_{\min}^{\text{pile}}+c_0^{\text{bat}}P_2^{\text{dis}}D_{\min}^{\text{pile}}+c_0^{\text{bat}}W_l^{\text{dh}}$.

xi) Egress arcs of charging or discharging $\text{A}_{\text{wait}}^{\text{pile}}$: Egress arcs describe the transition from a charging or discharging state to the waiting state at the depot. No energy variation occurs, $w\left(v_{\text{tra},t}^{\text{cha}},\ v_t^{\text{wait1}}\right)=w\left(v_{\text{bid},t}^{\text{cha}},\ v_t^{\text{wait1}}\right)=w\left(v_{\text{bid},t}^{\text{dis}},\ v_t^{\text{wait1}}\right)=0$ and $c\left(v_{\text{tra},t}^{\text{cha}},\ v_t^{\text{wait1}}\right)=c\left(v_{\text{bid},t}^{\text{cha}},\ v_t^{\text{wait1}}\right)=c\left(v_{\text{bid},t}^{\text{dis}},\ v_t^{\text{wait1}}\right)=0$.

2.2. Model formulation

For the E-VSP-BC, this paper considers the capacity limitations of unidirectional and bidirectional chargers at the depot and formulates an integer linear programming model, as shown in Eqs. (2) - (15). To support the economic and grid-friendly operations of EBs, the objective function is designed with two components. The first evaluates the operational costs and revenues associated with EB scheduling and V2G participation, where electricity purchase costs and battery degradation costs are treated as positive cost components, while discharging revenues are deducted from the objective. The second is the absolute deviation between the regulation energy provided by EBs and the regulation demand of the power grid. Accordingly, the objective value may become negative when the discharging revenues exceed the electricity purchase costs, battery degradation costs, and regulation deviation penalty costs considered in the model.

A binary variable $x_{k,i,j} \in \{0,\ 1\}$ is introduced to indicate whether EB k traverses arc $(i,\ j)$. A feasible path represents a continuous temporal sequence that captures trip connections (Call, 2010), deadheading movements, waiting decisions (Li et al., 2026c), charging and discharging operations (Liang et al., 2026), and battery energy evolution (Ding et al., 2026).

$$\min\ \text{Z}=\sum_{l\in\text{L}}\sum_{k\in\text{K}_l}\sum_{(i,j)\in\text{A}}c(i,j)x_{k,i,j}+\beta\sum_{f=1}^{F}\left(\delta_{1,f}^{+}+\delta_{2,f}^{+}+\delta_{1,f}^{-}+\delta_{2,f}^{-}\right) \quad (2)$$

$$\sum_{k\in\text{K}_l}\sum_{i:(i,j)\in\text{A}}x_{k,i,j}=1 \quad \forall j\in\text{V}_l^{\text{trip}},\ \forall l\in\text{L} \quad (3)$$

$$\sum_{j:(i,j)\in\text{A}_l^{\text{in}}}x_{k,o_l^{\text{in}},j}=1 \quad \forall k\in\text{K}_l,\ \forall l\in\text{L} \quad (4)$$

$$\sum_{i:(i,j)\in\text{A}_l^{\text{out}}}x_{k,i,o_l^{\text{out}}}=1 \quad \forall k\in\text{K}_l,\ \forall l\in\text{L} \quad (5)$$

$$\sum_{j:(i,j)\in\text{A}}x_{k,i,j}-\sum_{j:(i,j)\in\text{A}}x_{k,j,i}=0 \quad \forall i\in\text{V}\backslash\text{O}^{\text{vir}},\ \forall k\in\text{K}_l,\ \forall l\in\text{L} \quad (6)$$

$$\sum_{l\in\text{L}}\sum_{k\in\text{K}_l}\sum_{i:(i,j)\in\text{A}}x_{k,i,v_{\text{tra},t}^{\text{cha}}}\leq N \quad \forall t\in\text{T} \quad (7)$$

$$\sum_{l\in\text{L}}\sum_{k\in\text{K}_l}\sum_{i:(i,j)\in\text{A}}x_{k,i,v_{\text{bid},t}^{\text{cha}}}+\sum_{l\in\text{L}}\sum_{k\in\text{K}_l}\sum_{i:(i,j)\in\text{A}}x_{k,i,v_{\text{bid},t}^{\text{dis}}}\leq H \quad \forall t\in\text{T} \quad (8)$$

$$S_{k,j}Q_l=S_{k,i}Q_l+w(i,j)x_{k,i,j} \quad \forall(i,\ j)\in\text{A},\ \forall k\in\text{K}_l,\ \forall l\in\text{L} \quad (9)$$

$$S_{k,o_l^{\text{in}}}=S_l^{\text{sta}} \quad \forall k\in\text{K}_l,\ \forall l\in\text{L} \quad (10)$$

$$S_l^{\min}\leq S_{k,j}\leq S_l^{\max} \quad \forall j\in\text{V},\ \forall k\in\text{K}_l,\ \forall l\in\text{L} \quad (11)$$

$$\delta_{1,f}^{-}-\delta_{2,f}^{-}+P_1^{\text{cha}}\Delta t\sum_{l\in\text{L}}\left(\sum_{k\in\text{K}_l}\sum_{t=T_f^{\text{sta}}}^{T_f^{\text{end}}-\Delta t}x_{k,v_{\text{tra},t}^{\text{cha}},v_{\text{tra},t+1}^{\text{cha}}}+\sum_{k\in\text{K}_l}\sum_{t=T_f^{\text{sta}}}^{T_f^{\text{end}}-\Delta t}x_{k,v_{\text{bid},t}^{\text{cha}},v_{\text{bid},t+1}^{\text{cha}}}\right)=w_f^{-} \quad \forall f\in\text{F} \quad (12)$$

$$\delta_{1,f}^{+}-\delta_{2,f}^{+}+P_2^{\text{dis}}\Delta t\sum_{l\in\text{L}}\sum_{k\in\text{K}_l}\sum_{t=T_f^{\text{sta}}}^{T_f^{\text{end}}-\Delta t}x_{k,v_{\text{bid},t}^{\text{dis}},v_{\text{bid},t+1}^{\text{dis}}}=w_f^{+} \quad \forall f\in\text{F} \quad (13)$$

$$\delta_{1,f}^{-},\ \delta_{2,f}^{-},\ \delta_{1,f}^{+},\ \delta_{2,f}^{+}\in\mathbb{R}_{+} \quad \forall f\in\text{F} \quad (14)$$

$$x_{k,i,j}\in\{0,\ 1\} \quad \forall k\in\text{K}_l,\ \forall l\in\text{L},\ \forall(i,j)\in\text{A} \quad (15)$$

where β is the penalty coefficient for the deviation between the regulation energy of the EB fleet and the regulation demand of the power grid; $\delta_{1,f}^{-}$ and $\delta_{2,f}^{-}$ represent the shortfall and excess of downward regulation response in period f; $\delta_{1,f}^{+}$ and $\delta_{2,f}^{+}$ represent the shortfall and excess of upward regulation response in period f; $S_{k,i}$ and $S_{k,j}$ indicate the SOC of EB k at nodes i and j; S_l^{sta} gives the initial SOC of EBs serving route l at the beginning of the daily operation; $S_l^{\min}$ and $S_l^{\max}$ specify the minimum and maximum allowable battery SOC.

Constraint (3) imposes trip coverage, allowing each trip to appear in one and only one vehicle schedule. Constraints (4) and (5) require each EB to depart from the virtual origin of its assigned route and return to the corresponding virtual destination. Constraint (6) maintains flow conservation throughout the network by equating inflow and outflow at every node. Constraints (7) and (8) are depot capacity constraints that prevent conflicts in the use of unidirectional and bidirectional chargers. Constraints (9) tracks changes in battery SOC as EBs traverse different types of arcs. Constraint (10) sets the battery state at the start of daily operation, while constraint (11) requires the SOC to remain within the prescribed safe range over the entire scheduling horizon. Constraints (12) and (13) define the deviations between the charging and discharging energy and the corresponding regulation demand of the power grid in each period. Constraints (14) and (15) impose the admissible value ranges

Just Accepted

for the model variables.

2.3. Solution algorithm

The E-VSP-BC is a large-scale optimization problem (Tang et al., 2019), whose feasible solution space expands exponentially as the numbers of the number of routes (Cong et al., 2023), trips (Jiang and Zhang, 2022), and chargers. Directly solving the problem using a solver may make it difficult to obtain solutions within an acceptable computational time (Zhou et al., 2024). Given the strong route-level decomposability of the problem, this paper applies a column-generation-based diving heuristic, to efficiently obtain a high-quality solution. Specifically, the original formulation is decomposed into a restricted master problem (RMP) and pricing subproblems (PSP) (Ji et al., 2023). The RMP determines the combination of feasible scheduling schemes, while the PSP uses the dual information from the RMP to generate improving columns with negative reduced costs. After obtaining the linear relaxation solution, a diving heuristic (DH) is employed to construct an integer solution recursively, guided by high values in the fractional solution.

2.3.1. Column generation

The binary constraints in the original model, as formulated in Eqs (14) and (15), are first linearly relaxed. The trip coverage constraint in Eq. (3), the depot capacity constraints in Eqs. (7) and (8), and the regulation deviation constraints in Eqs. (12) - (13) are then treated as linking constraints. Dantzig-Wolfe decomposition is applied to formulate the RMP and the corresponding PSP. Since EBs serving the same route are homogeneous, they share the same feasible domain X_l. Let Ω_l denote the set of feasible scheduling schemes for route l. A continuous decision variable $y_{l,p}$ is defined to represent the number of EBs on route l that adopt scheduling scheme p, where $p \in \Omega_l' \subseteq \Omega_l$.

To describe the arc-flow information of each column and characterize its cost, trip coverage, and charger occupation, parameter $\hat{x}_{l,p,i,j} \in \{0,1\}$ is introduced. It equals 1 if feasible scheduling scheme p for route l traverses arc (i,j), and 0 otherwise. Accordingly, the cost $\tilde{c}_{l,p}$ of scheme p for route l is expressed as $\sum_{(i,j)\in \mathrm{A}} c_{i,j}\hat{x}_{l,p,i,j}$. The RMP is as follows:

$$\min\ \mathrm{Z} = \sum_{l\in \mathrm{L}}\sum_{p\in\Omega_l'} \tilde{c}_{l,p} y_{l,p} + \beta \sum_{f=1}^{F}\left(\delta_{1,f}^{+} + \delta_{2,f}^{+} + \delta_{1,f}^{-} + \delta_{2,f}^{-}\right) \tag{16}$$

$$\text{s.t.} \sum_{p\in\Omega_l'} a_{l,p,j}^{\mathrm{trip}} y_{l,p} = 1 \quad \forall j \in \mathrm{V}_l^{\mathrm{trip}},\ \forall l \in \mathrm{L} \tag{17}$$

$$\sum_{l\in \mathrm{L}}\sum_{p\in\Omega_l'} a_{l,p,t}^{\mathrm{tra}} y_{l,p} \le N \quad \forall t \in \mathrm{T} \tag{18}$$

$$\sum_{l\in \mathrm{L}}\sum_{p\in\Omega_l'} a_{l,p,t}^{\mathrm{bid}} y_{l,p} \le H \quad \forall t \in \mathrm{T} \tag{19}$$

$$P_1^{\mathrm{cha}}\Delta t \sum_{l\in \mathrm{L}}\sum_{p\in\Omega_l'} a_{l,p,f}^{-} y_{l,p} + \delta_{1,f}^{-} - \delta_{2,f}^{-} = w_f^{-} \quad \forall f \in \mathrm{F} \tag{20}$$

$$P_2^{\mathrm{dis}}\Delta t \sum_{l\in \mathrm{L}}\sum_{p\in\Omega_l'} a_{l,p,f}^{+} y_{l,p} + \delta_{1,f}^{+} - \delta_{2,f}^{+} = w_f^{+} \quad \forall f \in \mathrm{F} \tag{21}$$

$$\sum_{p\in\Omega_l'} y_{l,p} = K_l \quad \forall l \in \mathrm{L} \tag{22}$$

$$y_{l,p} \ge 0 \quad \forall p \in \Omega_l',\ \forall l \in \mathrm{L} \tag{23}$$

$$\delta_{1,f}^{-},\ \delta_{2,f}^{-},\ \delta_{1,f}^{+},\ \delta_{2,f}^{+} \ge 0 \quad \forall f \in \mathrm{F} \tag{24}$$

where K_l denotes the number of EBs assigned to route l; $a_{l,p,j}^{\mathrm{trip}}$ is trip coverage coefficient, $a_{l,p,j}^{\mathrm{trip}} = \sum_{(i,j)\in \mathrm{A}} \hat{x}_{l,p,i,j}$, and indicates whether feasible scheduling scheme p for route l covers trip node j; $a_{l,p,t}^{\mathrm{tra}}$ and $a_{l,p,t}^{\mathrm{bid}}$ are charger occupation coefficients, $a_{l,p,t}^{\mathrm{tra}} = \sum_{i:(i,j)\in \mathrm{A}} \hat{x}_{l,p,i,v_{\mathrm{tra},t}^{\mathrm{cha}}}$ and $a_{l,p,t}^{\mathrm{bid}} = \sum_{i:(i,j)\in \mathrm{A}} \hat{x}_{l,p,i,v_{\mathrm{bid},t}^{\mathrm{cha}}} + \sum_{i:(i,j)\in \mathrm{A}} \hat{x}_{l,p,i,v_{\mathrm{bid},t}^{\mathrm{dis}}}$, indicating whether scheme p for route l occupies unidirectional chargers and bidirectional chargers at time t; $a_{l,p,f}^{-}$ and $a_{l,p,f}^{+}$ are regulation deviation coefficients, characterizing the numbers of charging and discharging arcs generated by scheme p for route l in period f, $a_{l,p,f}^{-} = \sum_{t=T_f^{\mathrm{sta}}}^{T_f^{\mathrm{end}}-\Delta t} \hat{x}_{l,p,v_{\mathrm{tra},t}^{\mathrm{cha}},v_{\mathrm{tra},t+1}^{\mathrm{cha}}} + \sum_{t=T_f^{\mathrm{sta}}}^{T_f^{\mathrm{end}}-\Delta t} \hat{x}_{l,p,v_{\mathrm{bid},t}^{\mathrm{cha}},v_{\mathrm{bid},t+1}^{\mathrm{cha}}}$ and $a_{l,p,f}^{+} = \sum_{t=T_f^{\mathrm{sta}}}^{T_f^{\mathrm{end}}-\Delta t} \hat{x}_{l,p,v_{\mathrm{bid},t}^{\mathrm{dis}},v_{\mathrm{bid},t+1}^{\mathrm{dis}}}$.

Let $\pi_{l,j}$ denote the dual variable for the trip coverage constraint (17). Dual variables ψ_t^{tra} and ψ_t^{bid} correspond to the depot capacity constraints (18) and (19), while τ_f^{-} and τ_f^{+} are assigned to constraints (20) and (21). The fleet size constraint (22) is associated with σ_l. The reduced cost of column p for route l is given by Eq. (25), the constraints of the PSP is presented in Eqs. (26) - (32).

$$\begin{aligned}\min\ z' = & \sum_{(i,j)\in \mathrm{A}} c_{i,j}x_{i,j} - \sum_{j\in \mathrm{V}_l^{\mathrm{trip}}} \pi_{l,j} \sum_{i:(i,j)\in \mathrm{A}} x_{i,j} - \sum_{t\in \mathrm{TT}} \psi_t^{\mathrm{tra}} \sum_{i:(i,j)\in \mathrm{A}} x_{i,v_{\mathrm{tra},t}^{\mathrm{cha}}} \\ & - \sum_{t\in \mathrm{T}} \psi_t^{\mathrm{bid}} \sum_{i:(i,j)\in \mathrm{A}} \left(x_{i,v_{\mathrm{bid},t}^{\mathrm{cha}}} + x_{i,v_{\mathrm{bid},t}^{\mathrm{dis}}}\right) - P_1^{\mathrm{cha}}\Delta t \sum_{f\in \mathrm{F}} \tau_f^{-} \\ & \times \left(\sum_{t=T_f^{\mathrm{sta}}}^{T_f^{\mathrm{end}}-\Delta t} x_{v_{\mathrm{tra},t}^{\mathrm{cha}},v_{\mathrm{tra},t+1}^{\mathrm{cha}}} + \sum_{t=T_f^{\mathrm{sta}}}^{T_f^{\mathrm{end}}-\Delta t} x_{v_{\mathrm{bid},t}^{\mathrm{cha}},v_{\mathrm{bid},t+1}^{\mathrm{cha}}}\right) - P_2^{\mathrm{dis}}\Delta t \\ & \times \sum_{f\in \mathrm{F}} \tau_f^{+} \left(\sum_{t=T_f^{\mathrm{sta}}}^{T_f^{\mathrm{end}}-\Delta t} x_{v_{\mathrm{bid},t}^{\mathrm{dis}},v_{\mathrm{bid},t+1}^{\mathrm{dis}}}\right) - \sigma_l\end{aligned} \tag{25}$$

$$\text{s.t.} \sum_{j:(i,j)\in \mathrm{A}_l^{\mathrm{in}}} x_{o_l^{\mathrm{in}},j} = 1 \tag{26}$$

$$\sum_{i:(i,j)\in \mathrm{A}_l^{\mathrm{out}}} x_{i,o_l^{\mathrm{out}}} = 1 \tag{27}$$

$$\sum_{j:(i,j)\in A} x_{i,j} - \sum_{j:(j,i)\in A} x_{j,i} = 0 \quad \forall i \in \mathrm{V}\backslash \mathrm{O}^{\mathrm{vir}} \tag{28}$$

$$S_j Q_l = S_i Q_l + w(i,j) x_{i,j} \quad \forall (i,j) \in \mathrm{A} \tag{29}$$

$$S_{o_l^{\mathrm{in}}} = S_l^{\mathrm{sta}} \tag{30}$$

$$S_l^{\min} \le S_j \le S_l^{\max} \quad \forall j \in \mathrm{V} \tag{31}$$

$$x_{i,j} \in \{0,\ 1\} \quad \forall (i,j) \in \mathrm{A} \tag{32}$$

For route l, the PSP is essentially a resource-constrained shortest path problem (He et al., 2024). In this paper, it is solved using a label-setting (LS) algorithm. Specifically, labels are initialized at the virtual origin node. Each label records information such as the accumulated reduced cost, battery remaining energy, and predecessor label. The labels are extended along feasible arcs in the topological order of the time-expanded network, and each newly generated label is checked for resource feasibility. Labels that violate the lower or upper bound on battery energy, or any other resource constraints, are discarded. Each feasible label is then compared with the existing labels at the same node through dominance checks. If an existing label is no worse than the newly

Just Accepted

generated label, the new label is dominated and discarded. Conversely, if the new label is no worse than an existing label, the existing label is removed and the new label is retained. This process continues until all nodes have been processed. Finally, among the columns not yet appeared in RMP, the candidate with the lowest reduced cost is chosen for the RMP.

In the LS algorithm, dominance rules have a substantial impact on both computational efficiency and solution quality. To balance these two aspects, two dominance rules are designed:

Dominance rule I: This rule is relatively conservative and avoids discarding labels that may lead to an optimal solution. Specifically, for two labels A and B with the same remaining energy, label A dominates label B if the accumulated reduced cost of label A is no greater than that of label B. This rule helps preserve solution quality in the PSP. However, because the dominance condition is relatively weak, a large number of labels may be generated during the solution process, thereby reducing computational efficiency.

Dominance rule II: This rule discards inferior labels more aggressively while aiming to obtain high-quality solutions. Specifically, label A dominates label B if the accumulated reduced cost of label A is no greater than that of label B, the remaining energy of label A is no lower than that of label B, and label A is strictly better in at least one of these two dimensions. Compared with dominance rule I, dominance rule II can reduce the number of labels and accelerate the solution process (Jiang et al., 2023).

Dominance rule II is generally valid for the E-VSP-UC, but this property does not necessarily extend to the E-VSP-BC. Under V2G mode, remaining energy is not only a feasibility resource but also a flexible asset. In other words, it influences the feasibility, as well as the ability to provide upward or downward regulation of subsequent trips. Higher energy supports subsequent trips and discharging, while lower energy leaves more room for upward and downward regulation. As a result, neither a higher nor a lower energy is uniformly preferable, and the monotonicity assumption underlying dominance rule II no longer holds. Consequently, dominance rule II should not be used as the sole dominance criterion in the column-generation procedure. In this study, dominance rule II is first used to obtain an initial LP relation solution. The algorithm then switches to the more conservative dominance rule I and continues the column-generation iterations until no column can be generated. For clarity, the exclusive use of dominance rule I throughout the column generation is hereafter referred to as dominance strategy I, whereas the above two-stage strategy is referred to as dominance strategy II. The latter improves computational efficiency while ensuring the validity of the final lower bound.

2.3.2. Diving heuristic

The solution obtained by column generation is an LP relaxation solution and typically contains fractional variables. Therefore, it cannot be directly used as a feasible solution. A common approach is to incorporate a branch and bound (B&B) algorithm, leading to a branch and price (B&P) framework (Lu et al., 2026). This framework progressively eliminates fractional solutions and searches for the optimal integer solution. However, the problem considered here involves many candidate paths that are structurally similar and yield comparable contributions to the objective function. As a result, the B&P algorithm tends to exhibit slow convergence of the upper bound, which significantly hinders computational efficiency. The main reasons are as follows:

i) The fine-grained time discretization used in this paper creates a large number of charging, discharging, and waiting nodes, resulting in many similar arcs in the time-expanded network. This gives rise to a large number of nearly equivalent paths. Consequently, new columns generated by the PSP are often highly similar to existing ones. Even when these columns have negative reduced costs, they may contribute only marginal improvements in the LP relaxation objective value of the RMP.

ii) The objective function balances operating costs and regulation deviation, creating an inherent trade-off. Reducing regulation deviation may require EBs to charge or discharge during economically suboptimal periods, while prioritizing operating costs may limit the ability to meet grid regulation demands. As a result, improvements in the objective value tend to be gradual, further slowing the convergence of the algorithm.

To address this issue, this paper adopts the DH that exploits the structural information (Parmentier et al., 2023) embedded in the LP relaxation solution (Ma et al., 2026). It aims to rapidly construct a high-quality integer feasible solution within a relatively short computational time. Specifically, columns with the largest values of $y_{l,p}$ are selected as priority candidates for fixing. Meanwhile, the corresponding branches where they are fixed to 0 are stored as backtracking nodes. They can be revisited if the current search path fails to construct a feasible integer solution. In this way, the DH can efficiently extract promising path combinations from the fractional solution and obtain the integer feasible solution without exploring a large-scale branch tree.

3 Numerical experiments

3.1. Data and parameter setting

Two actual bus routes are selected to demonstrate the performance of the proposed model and algorithm. Routes 15 and 88 are selected, as they originate from the same depot. Route 88 covers 11.7 km with 22 stations in the inbound direction and 13.1 km with 23 stations in the outbound direction. Route 15 is 19.3 km long in each direction, with 34 stations arranged symmetrically. The departure stations of both routes are close to the depot. The deadheading time and distance are set to 3 min and 1 kWh.

A trip is defined as the process (Ji et al., 2026a) in which an EB departs from the origin station, completes both inbound and outbound services, and returns to the same terminal. For Route 15, the first and last trips depart at 06:00 and 18:30. The route operates 60 trips per day, with an average travel time of 134.7 min. Route 88 has a longer daily service period, from 04:50 to 22:00, with 144 trips per day and an average travel time of 98 min. Travel times of two routes are presented in Fig. 2.

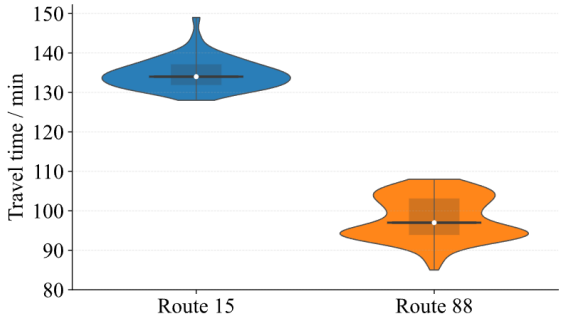


Fig. 2. Trip travel time for Routes 15 and 88.

A fleet of 13 EBs is assigned to Route 15 for daily operation.

Under Review

They have a curb weight of 17,900 kg and are equipped with batteries rated at 218.54 kWh. Route 88 is served by 20 EBs during the operation time, whose curb weight is 18,000 kg and battery rated capacity is 173 kWh. The allowable range of SOC for EB batteries is [20%, 100%]. The battery degradation cost (c_0^{bat}) per unit of energy throughout is set to 0.1 CNY/kWh. Trip energy consumption is estimated based on the approach introduced by Ji et al. (2022), where route length, travel time, and bus curb weight serve as input variables. The estimated average trip energy consumption is 27 kWh for Route 15 and 19 kWh for Route 88. The information about the two routes is summarized in Table 1.

Table 1. Detailed information about Routes 15 and 88

l	Route	$\lvert B_l \rvert$	$\lvert K_l \rvert$	Q_l (kWh)	Average travel time (min)	Average energy consumption (kWh)
1	15	60	13	218.54	134.7	27
2	88	144	20	173	98	19

The depot has two unidirectional chargers (i.e., N =2) and six bidirectional chargers (i.e., H =6). The charging power (P_1^{cha}) and the discharging power (P_2^{dis}) are 120 kW. The time-of-use charging and discharging prices, as well as the power grid regulation demands, are listed in Table 2. Given that a local V2G discharging pricing mechanism has not yet been implemented, price settings are determined by referring to real-world tariffs adopted in another city. Considering factors such as the availability of EBs, the number of unidirectional and bidirectional chargers, as well as their power, the upward and downward regulation energy demands are assumed in Table 2.

Table 2. Electricity prices and power grid regulation demands within periods

f	T_f^{sta}	T_f^{end}	c_f^{cha} (CNY /kWh)	c_f^{dis} (CNY /kWh)	w_f^+ (kWh)	w_f^- (kWh)
1	4:00	6:00	0.328	2	--	--
2	6:00	7:00	0.328	1	--	--
3	7:00	8:00	0.528	1	100	--
4	8:00	10:00	0.628	1	500	--
5	10:00	14:00	0.528	1	0	2,000
6	14:00	16:00	0.528	2	0	1,200
7	16:00	20:00	0.628	3	2,000	0
8	20:00	22:00	0.528	3	100	0

In addition, the time slot duration (Δt) is set to 1 min to capture the temporal evolution of charging and discharging activities. It allows the activity start and end times to be represented with sufficient accuracy, while maintaining a manageable size of the time-expanded network. The minimum charging or discharging duration ($D_{\min}^{\text{pile}}$) is required to be 15 min to avoid short charging/discharging operations. The penalty coefficient (α) for the deviation between the energy provided by the EB fleet and the power grid regulation demand is assigned a value of 1 CNY/kWh, which encourages the EB fleet to follow the regulation demand.

3.2. Result analysis

3.2.1. Optimization results under two dominance strategies

The algorithm is implemented in C++, and Gurobi 13.0 is adopted as the solver for the RMP. All numerical experiments are carried out on a computer with an Intel Core i7-12700H 2.30 GHz CPU and 16 GB RAM. As presented in Section 2.3.1, two dominance strategies are developed for solving the PSP. Based on this, the optimized vehicle and bidirectional charging scheduling schemes are presented in Fig. 3.

The solution obtained using dominance strategy I has an objective value of -4,436.4 CNY, comprising electricity purchase costs of 1,625.2 CNY, discharging revenues of 7,958.0 CNY, battery degradation costs of 1,086.4 CNY, and regulation deviation penalty costs of 810.0 CNY. In comparison, the solution obtained using dominance strategy II has an objective value of -4,407.7 CNY, including electricity purchase costs of 1,646.3 CNY, discharging revenues of 7,942.0 CNY, battery degradation costs of 1,094.0 CNY, and regulation deviation penalty costs of 794.0 CNY. Under both dominance strategies, the discharging revenues exceed the sum of electricity purchase costs, regulation deviation penalty costs, and battery degradation costs, resulting in a negative value. This finding shows that EB fleet participation in V2G can improve operational economic performance.

The solution obtained under dominance strategy I has an objective value 28.7 CNY lower than that under dominance strategy II. This improvement in solution quality is attributed to the more conservative dominance criterion of strategy I, which retains more labels with potential for future improvement and enables a more extensive exploration of the solution space. However, retaining more labels also increases the computational burden. The computation time under dominance strategy I is 2,978.8 s, whereas dominance strategy II requires only 1,798.4 s, reducing the computation time by approximately 39.6%. Overall, dominance strategy II is more suitable when computational efficiency is prioritized, whereas dominance strategy I is preferable when greater emphasis is placed on solution quality.

Just Accepted

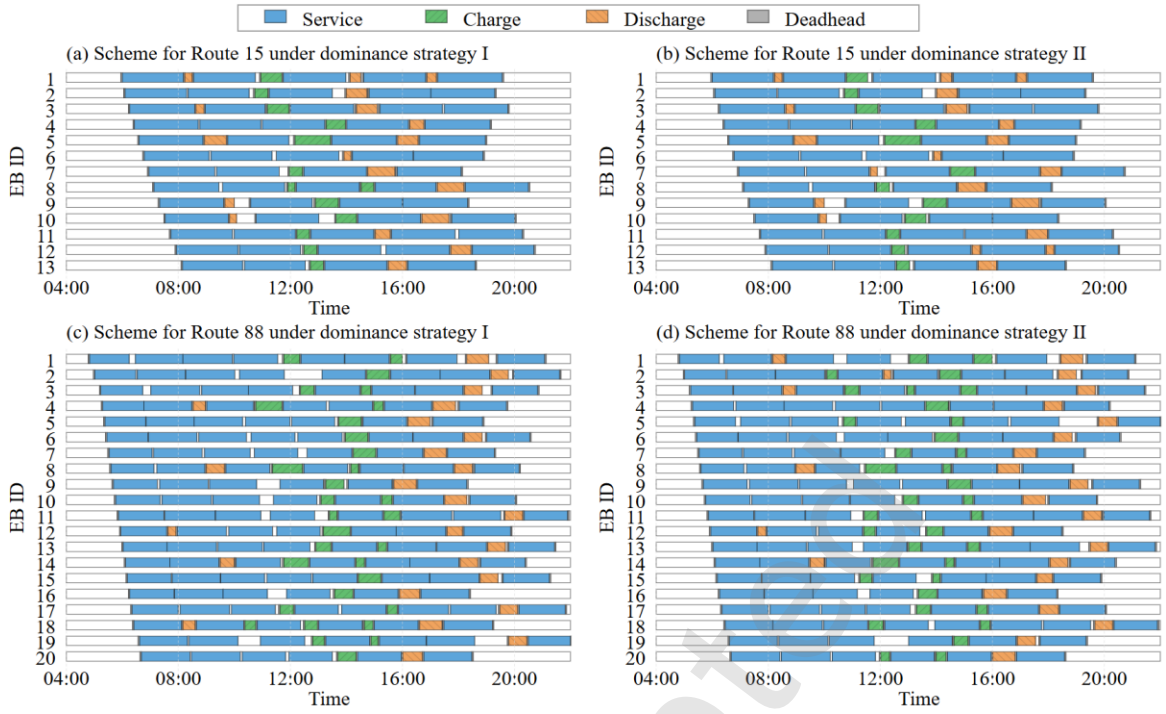


Fig. 3. Vehicle and bidirectional charging scheduling scheme based on two dominance strategies

The extent of the solution-quality loss under dominance strategy II depends largely on the scheduling conditions. It is expected to perform better when EBs have relatively long depot dwell times and charging/discharging resources are sufficient, as these conditions tend to generate more feasible labels with similar cost and energy states, so that discarding some of them is less likely to compromise solution quality. In contrast, short depot dwell times or tight charging/discharging resources would increase the likelihood that potentially valuable labels are discarded, thereby causing a greater loss in solution quality.

3.2.2. Fleet-level response to regulation demand

Fig. 4 compares the fleet charging and discharging energy with the regulation demand under two dominance strategies. The charging and discharging schemes generated based on both dominance strategies are grid-friendly. This demonstrates that the proposed method can effectively coordinate the bidirectional energy exchange while maintaining regular transit services. The satisfaction rates of the power grid regulation demand are 86.3% and 86.5% under the two dominance strategies, respectively. The downward regulation demand is relatively well satisfied, whereas deviations in the upward regulation demand are concentrated between 10:00 and 20:00. Furthermore, dominance strategy II provides a closer match to the downward regulation demand, while dominance strategy I performs better in responding to the upward regulation demand. The total charging energy of EBs under dominance strategy I is 122 kWh lower than the charging demand. Under dominance strategy II, the deviation is reduced to 82 kWh. In terms of discharging, the discharging energy under dominance strategy I is 20 kWh during period 10:00-14:00, when there is no discharging demand, which is substantially lower than 80 kWh under dominance strategy II. Meanwhile, its discharging deviations during periods 14:00-16:00 and 16:00-20:00 increase by 32 kWh and 4 kWh. The total discharging deviation under dominance strategy I is 24 kWh lower than that under dominance strategy II.

3.2.3. Vehicle-level charging and discharging characteristics

As shown by the vehicle-level charging and discharging energy in Fig. 5, the two routes exhibit distinct energy exchange characteristics. On Route 15, 11 EBs discharge more energy than they charge under both dominance strategies, indicating a stronger tendency to supply energy to the power grid. On Route 88, 16 and 15 EBs charge more energy than they discharge under dominance strategy I and dominance strategy II, respectively, reflecting a more pronounced energy replenishment pattern. The total charging and discharging energy on each route remains similar under the two dominance strategies. Changes in the dominance strategy have a limited effect on the vehicle-level energy exchange. Relative to the results under dominance strategy I, the charging and discharging energy under dominance strategy II of Route 15 increases by 18 kWh and 4 kWh, while those of Route 88 increase by 22 kWh and 20 kWh.

UBS Accepted

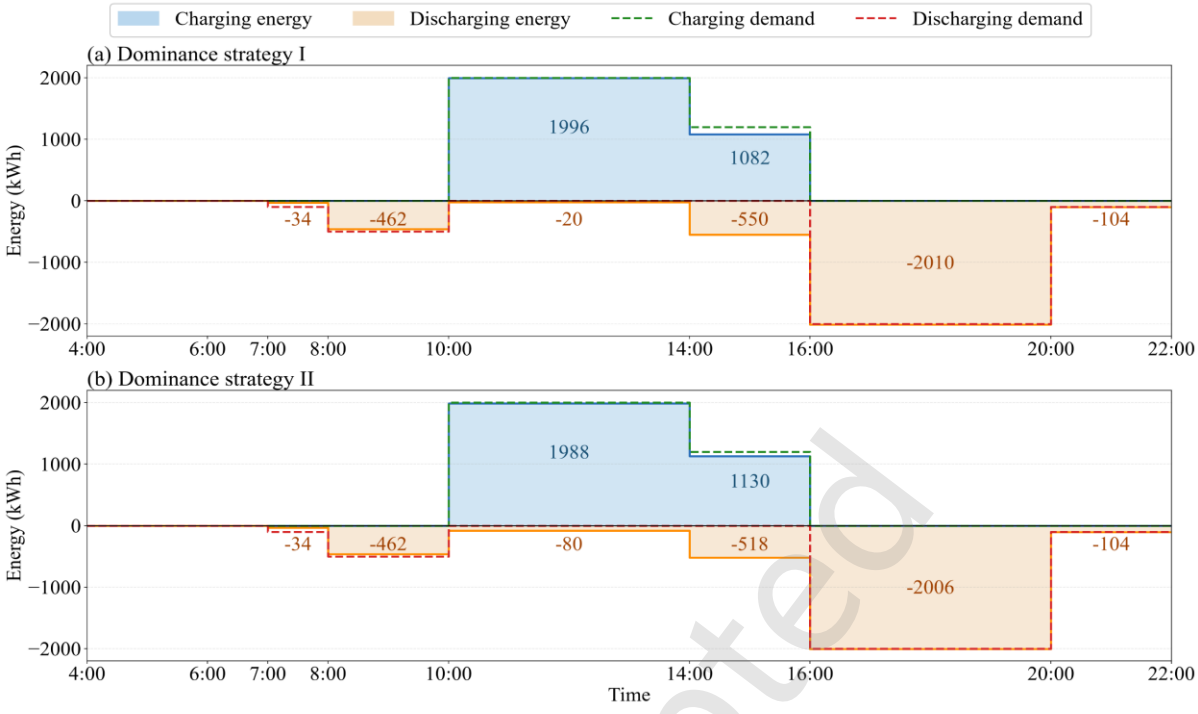


Fig. 4. Comparison of charging and discharging energy with regulation demand under different dominance strategies

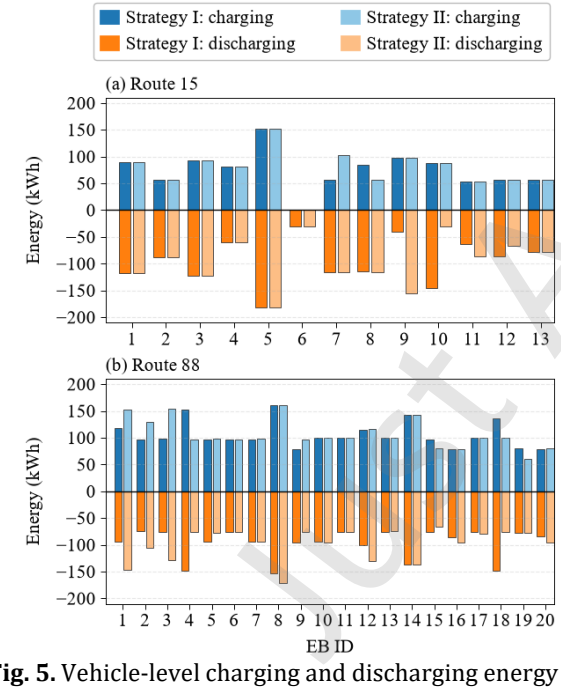


Fig. 5. Vehicle-level charging and discharging energy under different dominance strategies

By contrast, the choice of dominance strategy has a greater influence on the allocation of charging and discharging tasks among individual EBs. On Route 15, the adjustments are concentrated among a small number of EBs. The largest changes in discharging energy occur for EBs 9 and 10, with an increase and a decrease of 116 kWh, demonstrating a substantial transfer of discharging tasks between EBs. On Route 88, more EBs are affected, and the redistribution of charging and discharging tasks is more extensive. The proportions of EBs with changes in charging and discharging energy reach 60% and 75%. The sums of the absolute changes in vehicle-level charging and discharging energy on Route 88 are 278 kWh and 404 kWh.

3.3. Comparative analysis

3.3.1. Performance evaluation of the B&P and DH algorithms

The computational efficiency of the DH algorithm is further assessed against a B&P algorithm. Specifically, the DH is first used to generate an integer feasible solution, which provides the incumbent upper bound for the subsequent B&P procedure. The B&P algorithm then explores the B&B tree to seek further improvements. Since column generation need repeatedly executed at each search node, the B&P algorithm is computationally intensive, and its maximum runtime is limited to 7,200 s. For a fair comparison, both algorithms use the same RMP, PSP, and input parameters. The corresponding optimization results are reported in Table 3.

Table 3. Computational performance of B&P and DH algorithms

Algorithm	Dominance strategy	Objective value (CNY)	Gap (%)	Time (s)
B&P	Dominance strategy I	-4,437.6	0.36%	7,200
B&P	Dominance strategy II	-4,450.1	0.08%	7,200
DH	Dominance strategy I	-4,436.4	0.39%	2,978.8
DH	Dominance strategy II	-4,407.7	1.04%	1,798.4

Under dominance strategy I, the B&P algorithm reduces the optimality gap from 0.39% for the DH algorithm to 0.36%, corresponding to only a 1.2 CNY improvement in the objective value. However, its computation time reaches 7,200 s, approximately 2.42 times that of the DH algorithm. Under dominance strategy II, the advantage of B&P is more pronounced, reducing the optimality gap from 1.04% to 0.08%. However, the computation time is about four times that of the DH algorithm. The larger difference in solution quality between the two algorithms under dominance strategy II may

Just Accepted

be attributed to the effect of preliminary label filtering on the structure of the linear relaxation solution. Overall, although the B&P algorithm can improve the integer feasible solution by further exploring B&B nodes, only a marginal improvement in solution quality is achieved at the cost of a much longer computation time.

For larger multi-route EB systems, computational efficiency becomes increasingly important as the problem scale grows. The computational burden depends not only on the numbers of routes, trips, buses, and chargers, but also on their combined effects on scheduling flexibility and resource competition. The route-based decomposition provides a favorable structure for handling such growth, as the pricing problems are solved separately for individual routes, while the coupling among routes through shared depot resources is handled in the master problem.

3.3.2. Comparative analysis under cost-oriented scheduling

As described in Section 2.2, the proposed model minimizes operating costs and penalty costs associated with deviations from the power grid regulation demand, as formulated in Eq. (2). The corresponding deviations are defined by Eqs. (13) - (16). The model is designed to support economically and grid-friendly operations of the EB fleet. However, incorporating regulation demand may reshape the temporal distribution of charging and discharging activities and consequently change the economic benefits. To compare the original coordinated scheduling model with a cost-oriented scheduling model, this section constructs a comparative analysis. Specifically, the objective terms and constraints related to power grid regulation demands are removed, while input parameters are kept the same as those in Section 3.1. Dominance strategy I yields a lower objective value in the original model. Thus, the DH based on dominance strategy I is adopted for the solution.

Under the cost-oriented scheduling scenario, the operating costs are -5,589.5 CNY, representing a 6.54% reduction compared with the original model. Specifically, the discharging revenues increase by 592.0 CNY, while the electricity purchase costs and battery degradation costs increase by 159.7 CNY and 89.2 CNY. The increase in discharging revenues is greater than the increases in electricity purchase and battery degradation costs, indicating that the fleet can more flexibly participate in V2G and exploit peak-valley price arbitrage.

Further examination of the energy responses in Table 4 shows that, under the cost-oriented scheduling scenario, the total discharging energy decreases from 1,470.0 kWh in the original model to 1,290.0 kWh, even though the discharging revenue increases. This indicates that the cost reduction mainly results from the temporal reallocation of discharging activities rather than an increase in total discharging energy. Specifically, during periods 8:00-10:00 and 20:00-22:00, the discharging energy increases from 159.6 kWh and 11.1 kWh in the original model to 260.0 kWh and 40.5 kWh, respectively. By contrast, during period 10:00-14:00, the discharging energy decreases sharply from 288.5 kWh to 20.0 kWh, reflecting a clear temporal shift in discharging activities. Thus, removing regulation requirements allows more discharging activities to be shifted toward economically favorable periods.

Table 4. Comparison of fleet energy responses between the original and cost-oriented models

f	Original model			Cost-oriented model		
	w_f^+ (kWh)	w_f^- (kWh)	E_f^+ * (kWh)	E_f^- * (kWh)	E_f^+ * (kWh)	E_f^- * (kWh)
1	--	--	30	0	0	0
2	100	--	30	0	30	0
3	500	--	159.6	0	260	0
4	0	2,000	288.5	847.7	20	805.1
5	0	1,200	202.6	502.3	215.3	544.9
6	2,000	0	748.3	30	724.2	0
7	100	0	11.1	0	40.5	0
Total	2,700	3,200	1,470	1,380	1,290	1,350

Note: * E_f^+ is the discharging energy of EBs in period f; E_f^- is the charging energy of EBs in period f.

3.3.3. Comparative analysis under sufficient charging and discharging resources

In the multi-route system with a shared depot, depot capacity limitations directly affect the charging, discharging, and waiting arrangements of EBs, thereby restricting the flexibility of the EB fleet. To assess the effects of depot capacity limitations on the obtained scheduling solutions, this section constructs a comparative scenario with sufficient charging and discharging resources. In this scenario, the number of unidirectional chargers and bidirectional chargers that can be occupied simultaneously is no longer restricted, which is equivalent to removing the depot capacity constraints in the original model, as formulated in Eqs. (20) and (21). The model input parameters remain the same as those in Section 3.1, and dominance strategy I is also used in this section. A comparison is provided in Figs. 6 and 7.

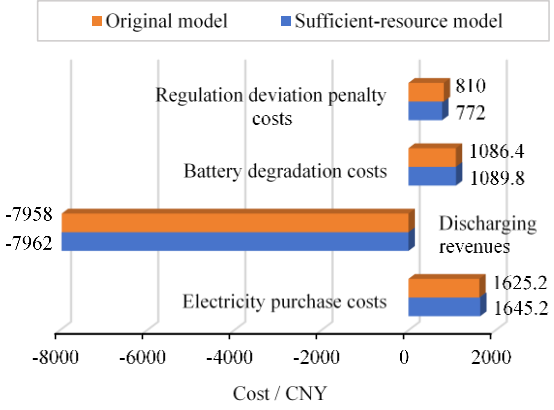


Fig. 6. Comparison of cost components between original and sufficient-resource models

Under the sufficient charging and discharging resource scenario, the objective value decreases by 18.6 CNY. As shown in Fig. 6, this improvement is mainly driven by a 38.0 CNY reduction in regulation deviation penalty costs. Although electricity purchase costs and battery degradation costs increase by 20.0 CNY and 3.4 CNY, these additional costs are offset by the reduction in regulation deviation penalty costs and the increase in discharging revenues. The sufficient charging and discharging resources enable the fleet to better respond to the power grid regulation demands.

Under Review

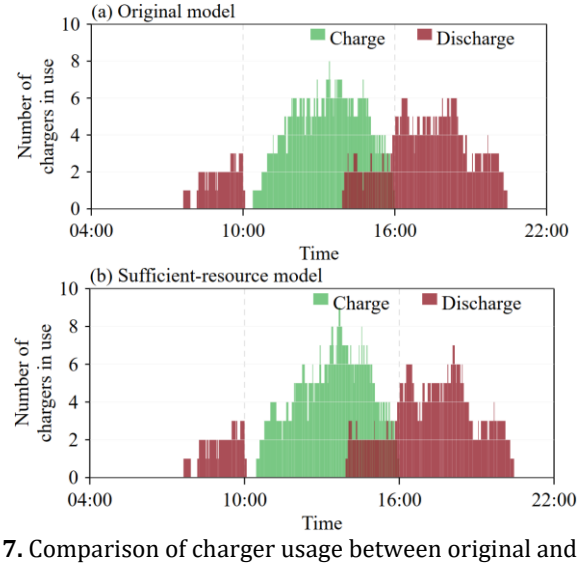


Fig. 7. Comparison of charger usage between original and sufficient-resource models

As demonstrated in Fig. 7, the maximum number of simultaneously occupied chargers is eight when depot capacity constraints are considered. Under the sufficient-resource scenario, this number increases to nine, exceeding the number of chargers given in Section 3.1. Therefore, removing depot capacity constraints may lead to infeasible charger usage in practice. These constraints are necessary to ensure scheduling scheme feasibility.

3.4. Sensitivity analysis

3.4.1. Impact of battery rated capacity

Battery capacity has a significant influence on the charging and discharging decisions of EBs in the proposed method. When battery rated capacities are relatively small, the available discharging energy is limited, and more frequent charging may be required to ensure the feasibility of subsequent trips, thereby restricting their ability to participate in regulation services. As battery rated capacity increases, EBs have greater energy reserves and can adjust scheme more flexibly in response to electricity prices and regulation demand. Therefore, this section conducts a sensitivity analysis of battery rated capacity. Only the capacity is varied, while other input parameters remain consistent with those in Section 3.1. The DH based on dominance strategy I is also adopted for the solution. On this basis, the impacts of different battery rated capacities on operating costs and regulation deviation penalty costs are analyzed, as presented in Fig. 8.

With larger battery capacities, EBs have more energy available and greater flexibility in coordinating charging and discharging operations, leading to a clear downward trend in operating costs. For example, when Route 15 EBs are equipped with 100 kWh batteries, increasing that of Route 88 from 90 kWh to 210 kWh reduces the system operating costs from 830.9 CNY to -4,007.1 CNY. When the battery rated capacity of Route 15 is further increased to 260 kWh, the system operating costs decrease to -7,074.6 CNY.

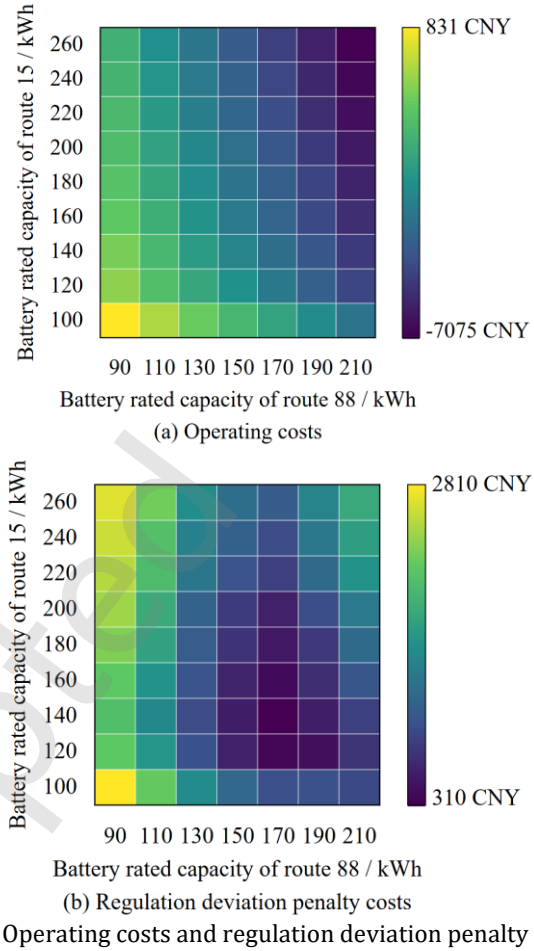


Fig. 8. Operating costs and regulation deviation penalty costs for different battery rated capacities

By contrast, the regulation deviation penalty costs do not decrease monotonically with battery rated capacity. Instead, they first decrease and then increase, reaching their minimum value of 310 CNY when the capacities of EBs on Routes 15 and 88 are 140 kWh and 170 kWh, respectively. Nevertheless, the increase in regulation deviation penalty costs observed in some high-capacity scenarios is outweighed by the corresponding reduction in operating costs. Therefore, V2G operation is more favorable for EB systems with relatively large battery capacities. However, this does not imply that transit operators should blindly select larger battery capacities, as the potential operating benefits should be balanced against the associated vehicle or battery acquisition costs.

3.4.2. Impact of the proportion of bidirectional chargers

The proportion of bidirectional chargers is a key infrastructure parameter that determines the available V2G service capacity at the depot. It directly affects the extent to which the EB fleet can participate in power grid regulation and obtain discharging revenue. Accordingly, a sensitivity analysis of the proportion of bidirectional chargers is developed. Keeping the total number of chargers unchanged, only proportion of bidirectional chargers is adjusted, and all other input parameters remain the same as those in Section 3.1. The DH based on dominance strategy I is also adopted for the solution. On this basis, the operating costs and regulation deviation penalty costs under different proportion scenarios are compared, as shown in Fig. 9.

Under Review

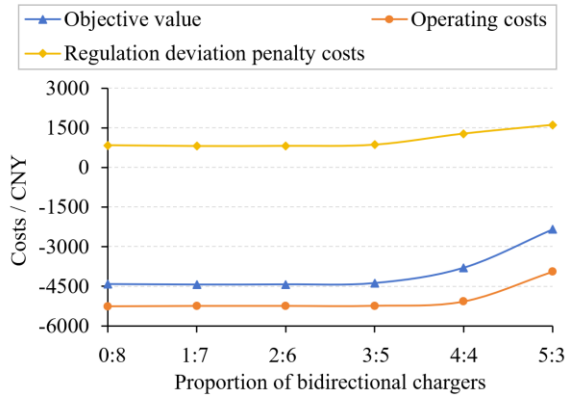


Fig. 9. Objective function decomposition under different proportions of bidirectional chargers

A reduction in the number of bidirectional chargers is generally accompanied by higher operating costs, indicating that a lower proportion of bidirectional chargers weakens the economic performance and grid-friendliness of the EB system. Specifically, when the number of bidirectional chargers decreases from eight to five, the operating costs change only slightly from -5,260.5 CNY to -5,242.7 CNY, and regulation deviation penalty costs increase from 836.0 CNY to 856.0 CNY. This suggests that, when bidirectional chargers are relatively sufficient, the system still has enough flexibility to absorb a moderate reduction in bidirectional chargers without a notable loss in economic performance. However, when the number of bidirectional chargers further falls to four or fewer, both costs increase more rapidly. For instance, reducing the number of such chargers from five to four increases the operating costs and regulation deviation penalty costs by 3.1% and 49.1%, respectively. When the number further decreases to three, the corresponding increases are 22.2% and 26.0%. Under these conditions, the ability of EBs to participate in regulation is significantly constrained, resulting in a rapid increase in both operating costs and regulation deviation penalty costs. Therefore, under limited depot capacity, the proportion of bidirectional chargers should not be too low. Sufficient bidirectional chargers should be maintained to ensure system economic performance and grid regulation responsiveness.

3.4.3. Impact of penalty coefficient β

The objective function in this paper consists of operating costs and regulation deviation penalty costs, with the latter determined by the regulation deviation and the corresponding penalty coefficient. Therefore, the value of the penalty coefficient affects the balance between operating economic performance and grid-friendliness. Accordingly, a sensitivity analysis of the penalty coefficient is conducted. Based on the benchmark parameters in Section 3.1, only the regulation deviation penalty coefficient is adjusted, while other input parameters are kept unchanged. The DH based on dominance strategy I is also adopted for solutions. The impact of the penalty coefficient on the objective value, operating costs, and regulation deviation penalty costs is analyzed, as shown in Fig. 10.

As the penalty coefficient increases from 0.1 to 1, the objective value rises from -5,416.3 CNY to -4,436.4 CNY, and the operating costs increase from -5,573.1 CNY to -5,246.4 CNY. Meanwhile, the regulation deviation decreases from 1,568 kWh to 810 kWh. These results indicate that a larger penalty coefficient encourages charging and discharging schemes to be more strongly aligned with power grid regulation demand, albeit at the expense of system economic performance. By contrast, when the penalty coefficient is smaller, the model tends to coordinates charging and discharging activities in response to electricity price signals, thereby reducing operating costs. Thus, the penalty coefficient should be selected according to the operational priority of the transit operator. A larger value is more suitable when greater emphasis is placed on grid regulation performance, whereas a smaller value may be adopted when reducing operating costs is the primary concern.

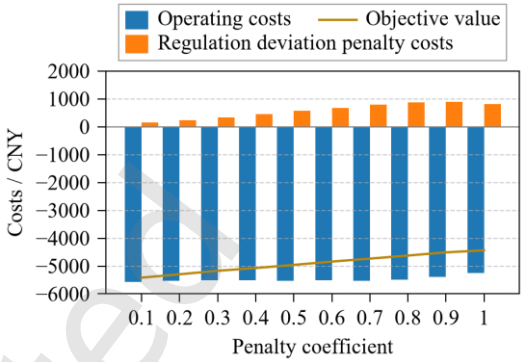


Fig. 10. Objective function decomposition under different penalty coefficients

4 Conclusions

This paper develops a coordinated optimization framework for V2G-enabled EB systems by jointly considering vehicle operations and bidirectional energy management. Based on a time-expanded network, a mixed-integer programming model with depot capacity constraints is formulated to coordinate trip assignment, charging decisions, and discharging decisions. A column-generation-based diving heuristic algorithm incorporating two dominance strategies is designed for the solution. The key results are outlined below.

i) The proposed method enhances the economic performance and grid-friendliness of the EB system. The optimized scheme has an objective value of -4,436.4 CNY, consisting of 1,625.2 CNY in electricity purchase costs, 7,958 CNY in discharging revenues, 1,086.4 CNY in battery degradation costs, and 810 CNY in regulation deviation penalty costs. The discharging revenue substantially offsets the charging and battery degradation costs, while EBs meet 86.3% of the power grid regulation demand without compromising the transit services.

ii) Solution quality and computational efficiency vary with the dominance strategy adopted. Compared with dominance strategy II, dominance strategy I achieves a lower objective value by 28.7 CNY, because its more conservative dominance criteria retain more potentially useful labels and allow a more comprehensive exploration of the solution space. However, the larger number of retained labels also increases the computational burden. By contrast, dominance strategy II reduces the computation time by approximately 39.6%, making it more suitable when computational efficiency is prioritized.

iii) Battery capacity, the proportion of bidirectional chargers, and the regulation deviation penalty coefficient are critical to balancing operational economy and grid-friendly performance. A larger rated battery capacity enhances operational economy, while sufficient bidirectional chargers are necessary to maintain regulation response capability. In addition, a higher penalty coefficient improves grid regulation tracking but may sacrifice economic benefits.

Just Accepted

Future work may enhance the proposed framework by accounting for uncertainties in energy consumption and grid regulation demand. In addition, more nonlinear battery degradation mechanisms and charging and charging power could also be considered to better evaluate the long-term impacts of V2G participation.

Author contributions

Yiming Bie: Writing – review & editing, Supervision, Methodology. **Yuman Xu:** Writing – original draft, Data curation, Methodology. **Ao Xue:** Software, Methodology, Formal analysis. **Jinhua Ji:** Writing – original draft, Methodology, Validation, Conceptualization, Funding acquisition. **Menglin Yang**: Formal analysis, Supervision. **Jue Zhou:** Methodology, Supervision, Conceptualization.

Replication and data sharing

The source code and replication package are available on ETS data at https://doi.org/10.26599/ETSD.2026.9190111.

Acknowledgements

This work was supported by the National Natural Science Foundation of China (grant numbers 72601189 and 72471102) and the Key Projects of National Natural Science Foundation of China (grant number 52220105001).

Declaration of competing interest

The authors have no competing interests to declare that are relevant to the content of this article.

References

Abdelwahed, A., van den Berg, P.L., Brandt, T., Collins, J., Ketter, W., 2020. Evaluating and optimizing opportunity fast-charging schedules in transit battery electric bus networks. Transportation Science, **54**(6), 1601–1615.

Bie, Y.M., Ji, Y.T., Ma, D.F., 2024. Multi-agent deep reinforcement learning collaborative traffic signal control method considering intersection heterogeneity. Transportation Research Part C: Emerging Technologies, **164**, 104663.

Brinkel, N., Zijlstra, M., van Bezu, R., van Twuijver, T., Lampropoulos, I., van Sark, W., 2023. A comparative analysis of charging strategies for battery electric buses in wholesale electricity and ancillary services markets. Transportation Research Part E: Logistics and Transportation Review, **172**, 103085.

Call, M., 2010. Inverse shortest path routing problems in the design of ip networks. Dissertation. Sweden, Linkopings Universitet.

Cong, Y., Wang, H.Q., Bie, Y.M., Wu, J.B., 2023. Double-battery configuration method for electric bus operation in cold regions. Transportation Research Part E: Logistics and Transportation Review, **180**, 103362.

Cong, Y., Bie, Y.M., Liu, Z.Y., Zhu, A.Z., 2024. Collaborative vehicle-crew scheduling for multiple routes with a mixed fleet of electric and fuel buses. Energy, **298**, 131400.

Cong, Y., Bie, Y.M., Wang, L.H., Xu, N., Yang, Y., 2025. Joint timetabling and vehicle formation design for autonomous modular buses under two-level route layout mode. IEEE Transactions on Intelligent Transportation Systems, **26**(10), 14690−14703.

Ding, Y.D., Wang, K., Zhang, W., Qu, X.B., 2026. Stochastic optimization of electric microtransit scheduling with platooning. Transportation Research Part B: Methodological, **209**, 103485.

Dong, G.P., Witlox, F., Bie, Y.M., 2024. Decentralizing e-bus charging infrastructure deployment leads to economic and environmental benefits. Communications in Transportation Research, **4**, 100139.

Gkiotsalitis, K., Iliopoulou, C., Kepaptsoglou, K., 2023. An exact approach for the multi-depot electric bus scheduling problem with time windows. European Journal of Operational Research, **306**(1), 189−206.

He, J., Yan, N., Zhang, J., Yu, Y., Wang, T., 2022. Battery electric buses charging schedule optimization considering time-of-use electricity price. Journal of Intelligent and Connected Vehicles, **5**(2), 138−145.

He, X., Yang, Z., Fan, T., Gao, J., Zhen, L., Lyu, J., 2024. Branch and price algorithm for route optimization on customized bus service. Annals of Operations Research, **335**(1), 205-236.

Huang, D., Li, F., Yin, J., Zhou, Y., Bie, Y., Wang, H., Liu, Z., 2026. Evolution of electric bus systems: A review of models, methods, and future directions. Transportation Research Part D: Transport and Environment, **157**, 105387.

Jahic, A., Plenz, M., Eskander, M., Schulz, D., 2021. Route scheduling for centralized electric bus depots. IEEE Open Journal of Intelligent Transportation Systems, **2**, 149−159.

Ji, J.H., Bie, Y.M., Zeng, Z.L., Wang, L.H., 2022. Trip energy consumption estimation for electric buses. Communications in Transportation Research, **2**, 100069.

Ji, J.H., Bie, Y.M., Wang, L.H., 2023. Optimal electric bus fleet scheduling for a route with charging facility sharing. Transportation Research Part C: Emerging Technologies, **147**, 104010.

Ji, Y.T., Bie, Y.M., Ma, D.F., 2026b. Dynamic charging optimization for electric buses under photovoltaic-storage-grid energy supply mode. Transportation Research Part C: Emerging Technologies, **184**, 105539.

Ji, J.H, Wang, L.H, Bie, Y.M, Li, S.W., 2026a. Economic and environmental analysis for electric bus system with dynamic wireless charging. Transportation Research Part D: Transport and Environment, **151**, 105159.

Jia, Z.N., An, K., 2025. Multi-depot battery electric bus scheduling and charging coordination under resource limitations. Applied Energy, **398**, 126444.

Jiang, M.Y., Zhang, Y., Zhang, Y., 2022a. A branch-and-price algorithm for large-scale multidepot electric bus scheduling. IEEE Transactions on Intelligent Transportation Systems, **24**(12), 15355−15368.

Jiang, M.Y., Zhang, Y., Zhang, Y., 2022b. Electric bus scheduling considering limited charging facility capacity for large-scale operation. Journal of Transportation Engineering, Part A: Systems, **148**(9), 04022058.

Kang, M., Lee, B., Lee, Y., 2025. A robust optimization approach for e-bus charging and discharging scheduling with vehicle-to-grid integration. Mathematics, **13**(9), 1380.

Ke, B.R., Lin, Y.H., Chen, H.Z., Fang, S.C., 2020. Battery charging and discharging scheduling with demand response for an electric bus public transportation system. Sustainable Energy Technologies and Assessments, **40**, 100741.

Lacombe, R., Murgovski, N., Gros, S., Kulcsár, B., 2024. Integrated charging scheduling and operational control for an electric bus network. Transportation research part E: logistics and transportation review, **186**, 103549.

Li, T.T., Zeng, X.Q., Qi, X., Zhao, T.Y., Li, Z.M., Lv, Y., 2025. Economical vehicle-side strategies for an electric bus charging station in vehicle-to-grid services based on reinforcement learning. Green Energy and Intelligent Transportation, **2025**, 100387.

Just Accepted

Li, Y.X., Zhong, Y.G., Qiu, Z.M., Cheng, T., 2026a. Promoting vehicle-to-grid deployment: Should subsidies target bidirectional charging station construction or operation? Transportation Research Part E: Logistics and Transportation Review, **211**, 104877.

Li, Z.X., Sai, Q., Wang, Y.X., 2026b. Optimal scheduling of electric bus fleets considering battery degradation effects. World Electric Vehicle Journal, **17**(4), 174.

Li, L., Liang, J., Zhuang, C., Gao, Z., Bao, Y., 2026c. A novel dynamic programming approach for minimum fleet size in electric bus transit lines. European Journal of Operational Research, DOI: 10.1016/j.ejor.2026.08.018.

Lian, Y., Lucas, F., Sörensen, K., 2023. The electric on-demand bus routing problem with partial charging and nonlinear function. Transportation Research Part C: Emerging Technologies, **157**, 104368.

Liang, J., Zhuang, C., Liu, H., Gao, Z., 2026. Demand-driven timetabling and vehicle scheduling optimization for electric bus transit lines. Transportation Research Part C: Emerging Technologies, **183**, 105482.

Lu, C.C., Yen, Y.C., Chien, Y.S., 2026. Optimizing urban bus operations during fleet electrification: A mixed fleet scheduling model with a column generation algorithm. Journal of Public Transportation, **28**, 100179.

Ma, N., Tang, A., Li, Y., Zhang, W., Jiang, F., Chen, Z., 2026. Column generation-based diving heuristic and segmentation approach for the micro-service allocation problem with affinity in cloud computing. Operational Research, **26**(2): 28.

Manzolli, J.A., Trovao, J.P.F., Antunes, C.H., 2022. Electric bus coordinated charging strategy considering V2G and battery degradation. Energy, **254**, 124252.

Najafi, A., Gao, K., Wang, H., Jasinski, M., Parishwad, O., Cui, S.H., 2025. Joint charging scheduling of electric buses and active power flexibility integration. Transportation Research Part E: Logistics and Transportation Review, **197**, 104038.

Othman, K., Da Silva, D., Shalaby, A., Abdulhai, B., 2025. Interpretable machine learning models for predicting Ebus battery consumption rates in cold climates with and without diesel auxiliary heating. Green Energy and Intelligent Transportation, **4**(2), 100250.

Parmentier, A., Martinelli, R., Vidal, T., 2023. Electric vehicle fleets: Scalable route and recharge scheduling through column generation. Transportation Science, **57**(3), 631-646.

Qiu, Z.Y., Hu, X.W., An, S., 2026. Robust collaborative scheduling optimization for multiple electric bus routes under stochastic traffic conditions. Transportation Research Part C: Emerging Technologies, **182**, 105455.

Sagaria, S., van der Kam, M., Boström, T., 2025. Vehicle-to-grid impact on battery degradation and estimation of V2G economic compensation. Applied Energy, **377**, 124546.

Shaheen, H.I., Rashed, G.I., Yang, B., Yang, J., 2024. Optimal electric vehicle charging and discharging scheduling using metaheuristic algorithms: V2G approach for cost reduction and grid support. Journal of Energy Storage, **90**, 111816.

Shirazi, Y., Carr, E., Knapp, L., 2015. A cost-benefit analysis of alternatively fueled buses with special considerations for V2G technology. Energy Policy, **87**, 591–603.

Son, J., Im, J., Kim, D., 2025. Urban transit optimization: Efficient electric bus operations and vehicle-to-grid integration. Computers & Industrial Engineering, **205**, 111169.

Tang, X.D., Lin, X., He, F., 2019. Robust scheduling strategies of electric buses under stochastic traffic conditions. Transportation Research Part C: Emerging Technologies, **105**, 163–182.

Tang, C.Y., Xue, H., Ceder, A., Ge, Y.E., 2024. Optimal variable vehicle scheduling strategy for a network of electric buses with fast opportunity charging. Transportmetrica A: Transport Science, **20**(3), 2182611.

Teng, J., Chen, T., Fan, W., 2020. Integrated approach to vehicle scheduling and bus timetabling for an electric bus line. Journal of Transportation Engineering, Part A: Systems, **146**(2), 04019073.

Wang, X.D., Song, Z.Q., Xu, H.L., Wang, H., 2023. En-route fast charging infrastructure planning and scheduling for battery electric bus systems. Transportation Research Part D: Transport and Environment, **117**, 103659.

Wang, W.S., Yu, B., Zhou, Y., 2024. A real-time synchronous dispatching and recharging strategy for multi-line electric bus systems. Transportation Research Part E: Logistics and Transportation Review, **185**, 103516.

Whitaker, J., Droge, G., Hansen, M., Mortensen, D., Gunther, J., 2023. A network flow approach to battery electric bus scheduling. IEEE Transactions on Intelligent Transportation Systems, **24**(9), 9098–9109.

Xiong, J., Bai, C.Y., Guan, W., Chen, Y.Y., Xu, Y., 2022. Mixed optimization on vehicle scheduling and recharge scheduling of plug-in electric buses with consideration of partial recharge. Journal of Transportation Engineering, Part A: Systems, **148**(2), 04021111.

Xu, X.M., Yu, Y.H., Long, J.C., 2023. Integrated electric bus timetabling and scheduling problem. Transportation Research Part C: Emerging Technologies, **149**, 104057.

Yao, B.Z., Qi, Z.H., Liu, Z.Q., Zhu, M.K., Cui, S.H., Precup, R.E., et al., 2025. Evaluating the sustainability of electric buses during operation via field data. Journal of Intelligent and Connected Vehicles, **8**(3), 9210061.

Yang, S.X., Wang, X.F., Ning, W.Q., Jia, X.F., 2021. An optimization model for charging and discharging battery-exchange buses: Consider carbon emission quota and peak-shaving auxiliary service market. Sustainable Cities and Society, **68**, 102780.

Zeng, Z.L., Qu, X.B., 2023. What's next for battery-electric bus charging systems. Communications in Transportation Research, **3**, 100094.

Zeng, Z.L., Wang, S.A., Qu, X.B., 2023. Consolidating bus charger deployment and fleet management for public transit electrification: A life-cycle cost analysis framework. Engineering, **21**, 45–60.

Zeng, Z.L., Wang, T.S., Qu, X.B., 2024. En-route charge scheduling for an electric bus network: Stochasticity and real-world practice. Transportation Research Part E: Logistics and Transportation Review, **185**, 103498.

Zhang, L., Han, Y., Peng, J.K., Wang, Y.D., 2023. Vehicle and charging scheduling of electric bus fleets: A comprehensive review. Journal of Intelligent and Connected Vehicles, **6**(3), 116–124.

Zhang, L., Wang, Y.D., Gu, W.H., Han, Y., Chung, E.D., Qu, X.B., 2024a. On the role of time-of-use electricity price in charge scheduling for electric bus fleets. Computer-Aided Civil and Infrastructure Engineering, **39**(8), 1218–1237.

Zhang, M.Y., Yang, M., Li, Y., Huang, S.Y., 2024b. Optimization of electric bus scheduling considering charging station resource constraints. Transportation Research Record, **2678**(3), 13–23.

Zhao, Y., Chen, X.Y., Liu, P., Nielsen, C.P., Mcelroy, M., 2025. Future ultrafast charging stations for electric vehicles in

Just Accepted

China: Charging patterns, grid impacts and solutions, and upgrade costs. Engineering, **48**, 309-322.

Zheng, Z., Li, J.X., Li, H.K., Zhu, Q., Liu, W.Q., Dong, D.W., 2026. Vehicle-to-grid capability and economic analysis of electric school buses under high-frequency trips through scheduling optimization. Journal of Energy Storage, **155**, 121365.

Zhou, Y., Wang, H., Wang, Y., Yu, B., Tang, T., 2024. Charging facility planning and scheduling problems for battery electric bus systems: A comprehensive review. Transportation Research Part E: Logistics and Transportation Review, **183**, 103463.

Zhou, F., Arvidsson, A., Wu, J., Kulcsár, B., 2024. Collaborative electric vehicle routing with meet points. Communications in Transportation Research, **4**, 100135.

Zhou, W., Chen, H.Y., Huang, P., Ma, Z.L., 2025a. Integrated operation and charging controls for ride-sharing electric autonomous mobility-on-demand systems. Journal of Intelligent and Connected Vehicles, **8**(4), 9210071.

Zhou, X.Y., An, K., Schmöcker, J.D., 2025b. Optimization of charging and discharging schedules for battery electric buses under the V2G environment. Transportmetrica B: Transport Dynamics, **13**(1), 2506689.

Author biography



Yiming Bie received the Ph.D. degree in Traffic Engineering from Jilin University, China. He is a Professor at School of Transportation, Jilin University. His research interests include smart transit operations, truck delivery, and low-altitude control and management.



Yuman Xu received the M.E. degree from Civil Aviation University of China. She is pursuing her Ph.D. degree at School of Transportation, Jilin University. Her research interests include smart and electrified transportation operations and vehicle-grid interaction.



Ao Xue received the B.S. degree in Traffic Engineering from Jilin University, China. He is pursuing his M.E. degree at School of Transportation, Jilin University. His research interests include vehicle-grid interaction and truck delivery.



Jinhua Ji received the Ph.D. degree in Vehicle Operation Engineering from Jilin University, China. She is currently a postdoctoral researcher at Jilin University. Her research interests include smart and electrified transportation operations and vehicle-grid interaction.



Menglin Yang received the Ph.D degree in Transportation Engineering from Southeast University, China. She is a postdoctoral researcher at Technische Universität Dresden, Germany. Her research interests include traffic control and the operation of electrified transportation systems.



Jue Zhou received the Ph.D. degree in Management Science and Engineering from Hefei University of Technology, China. He is an Associate Professor at School of Transportation, Jilin University. His research interests include transportation organization, operations research, and optimization methods.

Just Accepted